Journal of Electronic Testing (2022) 38:21–38
https://doi.org/10.1007/s10836-022-05988-y

Revisit to Histogram Method for ADC Linearity Test: Examination of Input Signal and Ratio of Input and Sampling Frequencies

Yujie Zhao[1] · Kentaroh Katoh[1] · Anna Kuwana[1] · Shogo Katayama[1] · Jianglin Wei[1] · Haruo Kobayashi[1] · Takayuki Nakatani[1] · Kazumi Hatayama[1] · Keno Sato[2] · Takashi Ishida[2] · Toshiyuki Okamoto[2] · Tamotsu Ichikawa[2]

Received: 7 September 2021 / Accepted: 18 February 2022 / Published online: 9 March 2022

Abstract
This paper revisits histogram method for ADC linearity test. Here two methods are proposed for low cost test of histogram method. The first proposal is two-tone sine wave input for code selective histogram method for SAR ADC. In SAR ADC, the DNL of the codes corresponding to the internal DAC output voltages of the MSB bits can be large when the DAC employs a binary-weighted configuration. Therefore, in the proposed method, frequency of appearance of the codes is increased to make the length of the bins relatively long with two-tone sine wave input. It realizes low cost test and high-quality linearity test. The 2nd proposal is decision method of the ratio of the input and sampling frequencies with classical number theory. The proposed method decides the ratio based on metallic ratio or theory of prime numbers. This guarantees random data sampling to get accurate calibration result with relatively small number of histogram data.

Keywords Code Selective Method · Histogram Method · Linearity Test · Mettalic Ratio Sampling · SAR ADC · Two-Tone

1 Introduction

In recent years, Internet of Things (IoT) has attracted much attention. For IoT-related ADCs high quality and rapid linearity testing has become more important at mass production shipping stage for keeping IoT system's quality and reliability.

The histogram method for ADC linearity test is widely used in industry [1–8]. Unfortunately, histogram tests take a relatively long time and sometimes are often omitted at the mass production shipping stage. However, due to recent demands for higher reliability in IoT systems and automotive applications, ADC linearity test is required, but low cost test is essential.

Various methods for test time reduction of ADC linearity test have been proposed [9, 10]. Chen et al. proposed the segmented non-parametric model, a model-based method [11, 12]. Laraba et al. proposed reduced-code linearity test for pipeline ADC [13]. This method reduces the static test time utilizing the fact that there exist different output transitions between consecutive codes that are due to the same comparator being exercised in one of the pipeline stages [14]. Regarding to SAR ADC linearity test, Feitoza et al. proposed reduced-code linearity tests for the different DAC architectures [15, 16]. These methods perform major carrier transition (MCT)-based test methodology with extra behaviors for the test. Huang et al. also proposed an MCT test-based approach characterizing the static linearity of a capacitive SAR ADC [17]. These methods for SAR ADC require extra area for extra behavior for the on-chip BIST implementation. On the other hand, because our method is histogram test-based approach, extra hardware is not required.

In this paper, we revisit histogram method for ADC linearity test. Here two methods are proposed for low cost test of histogram approach. The first proposal is two-tone sine

Responsible Editor: S. Mir

✉ Yujie Zhao
t202d002@gunma-u.ac.jp

Anna Kuwana
kuwana.anna@gunma-u.ac.jp

Haruo Kobayashi
koba@gunma-u.ac.jp

[1] Division of Electronics and Informatics, Faculty of Science and Technology, Gunma University, 1-5-1 Tenjin-cho, Kiryu-shi, Gunma 376-8515, Japan

[2] ROHM Co, Ltd, 2-4-8 Shin-Yokohama, Kohokuku, Yokohama 222-857, Japan

wave input for code selective histogram method for SAR ADC. In SAR ADC, the DNL of the codes corresponding to the internal DAC output voltages of the MSB bits can be large when the DAC employs a binary-weighted architecture. Therefore, in the proposed method, frequency of appearance of the codes is increased to make the length of the bins relatively long with two-tone sine wave input. It realizes low cost test and high-quality linearity test of MSB bits. The 2nd proposal is decision method of the ratio of the input and sampling frequencies with classical number theory. The proposed method decides the ratio based on metallic ratio or theory of prime numbers. This guarantees random data sampling to get accurate calibration result with relatively small number of histogram data.

The rest of the paper is organized as follows. Section 2 describes the basics of the histogram method. Section 3 explains the two-tone sine wave input for code selective histogram method, which is the first proposal. Section 4 explains decision of the ratio between input and sampling frequencies based on classical number theory, which is the 2nd proposal. Finally, Sect. 5 provides the conclusion.

2 Basics of Histogram Method

The histogram method offers quantitative estimates of ADC non-linearity by statistically processing the output samples. The ADC output samples are obtained by the input amplitude distribution (or probability density function) of the known input signal to the ADC [4–7].

Figure 1 explains differential nonlinearity (DNL) measurements with the saw input. Figure 1(a) shows that if the ADC is perfectly linear, the histogram shows identical bins. Figure 1(b) shows the case that the ADC has some non-linearity: DNL for each bin can be obtained from the corresponding histogram value and integral nonlinearity (INL) is calculated by accumulating DNLs for each code. Thus, by using the histogram method, both DNLs and INLs are determined with an accuracy that is proportional to the number of samples stored in each code.

Notice that the circuit noises are generated inside the ADC under the test, and hence the ADC digital outputs can vary even for the same analog input, which degrades ADC linearity tests such as using the servo loop method. However, the histogram method can average out this effect [2, 3].

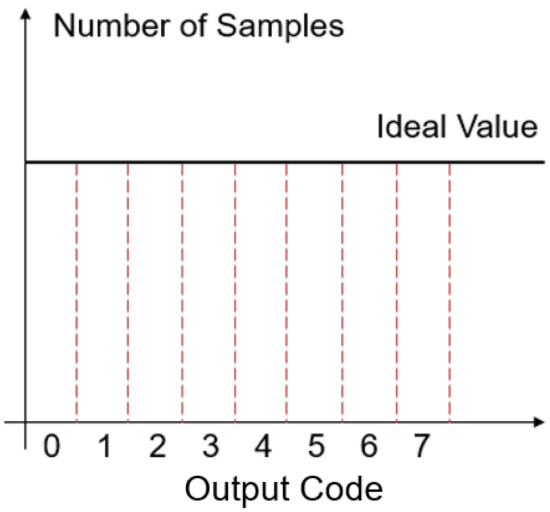

(a) Histogram of ADC output without non-linearity.

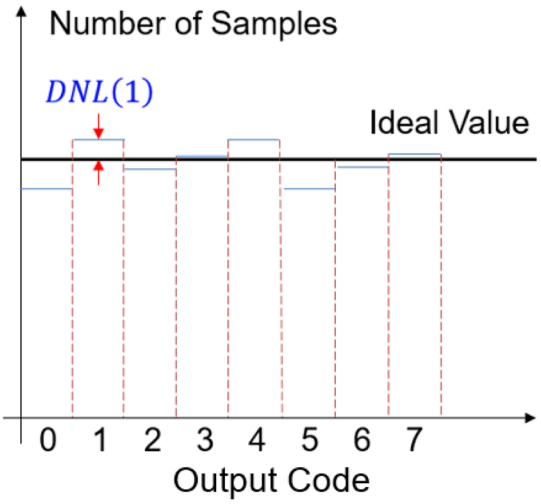

(b) Histogram of ADC output with non-linearity.

Fig. 1 ADC output histogram for saw input

3 Two-Tone Sine Wave Input for Code Selective Histogram Method

Here, code selective histogram method using two-tone sine wave input is explained, which is the first proposal. This is the method for SAR ADC linearity test. Subsection 3.1 briefly explains the basics of SAR ADC. This method is the extended method of the histogram method using sine wave input. Subsection 3.2 briefly explains the histogram method using sine wave input. Subsection 3.3 describes the proposed code selective histogram method using two-tone sine wave input. Subsection 3.4 shows the simulation results.

3.1 SAR ADC

Basics of SAR ADC is overviewed with Fig. 2. SAR ADC converts analog input to digital output using the binary search and comparing the sampled analog voltage to the DAC output voltage.

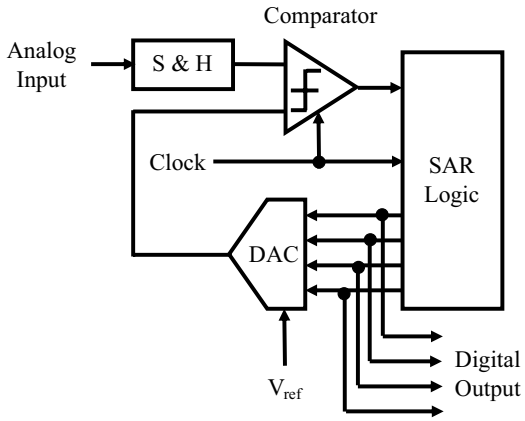

Fig. 2 Block diagram of typical SAR ADC

In many cases, the linearity of the DAC inside the ADC determines the linearity of the entire ADC. For example, in the 5-bit R-2R trapezoidal binary weighted DAC shown in Fig. 3, the largest nonlinearity is likely to occur near the digital codes 15 to 16 (all switches will change). Next, large nonlinearities may occur around 8, 24, and then around 4, 12, 20, and 28. The DAC codes prone to nonlinearity depend on the DAC architecture as shown in [18, 19].

3.2 Sine Wave Histogram Method

Now let us consider the sine wave histogram method. As shown in Fig. 4, the input sine wave is sampled and the histogram value of the corresponding digital output code bin is incremented by 1. Then, as shown in Fig. 5, the histogram or frequency of occurrence of each code can be plotted.

The horizontal axis of Fig. 5 corresponds to the amplitude (vertical axis) of input signal in Fig. 4. For example, in the case of a 12-bit ADC, the amplitude of the input signal is divided by 4096. Notice that it is relatively easy to achieve low distortion sine waves using analog filters [20, 21], though a highly linear saw signal is difficult to generate.

However, as shown in Fig. 5, the histogram is concentrated on both ends of the code, which is a disadvantage in

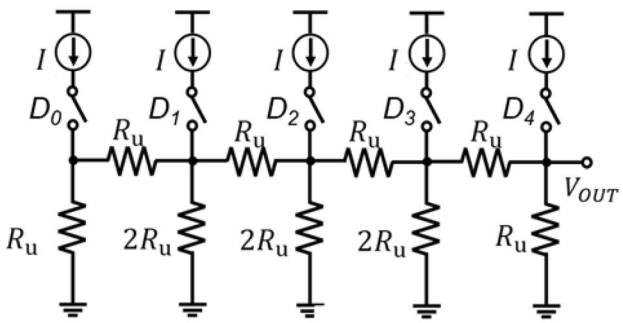

Fig. 3 R-2R ladder network DAC

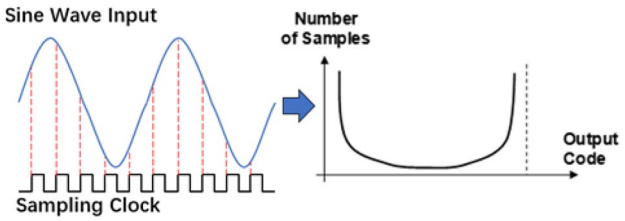

Fig. 4 Histogram generation for sine wave input

that the test time near the center code is relatively long. In many cases, ADC linearity must often be assured around the center code. Since DNL measurement accuracy is proportional to the number of data samples in the bin, histogram ADC testing with the sine wave input takes long time to measure the linearity accurately around the center of the ADC output range. However, focusing on specific codes can avoid this shortcoming, as shown in our previous study [22].

3.3 Two-Tone Sine Wave Input for Histogram Test of SAR ADC

We assume here that the target SAR ADC under test has a binary-weighted DAC inside. For example, in case of a 10-bit device, the DNL of the SAR ADC can be large at the digital codes of 512, 256, 768, 128, 384, 640, 896, … In other words, DNL can be large at the codes which corresponds to the DAC output voltage of MSB bits. Hence, we need to test their DNLs accurately, and when the histogram test is employed, the input signal should be synthesized so that the histogram is heavily weighted at these codes.

In this paper, the two-tone sine wave is expressed as the following equation:

$$f_{\omega_2}(t) = \sin(\omega_1 t) - \frac{\sin(\omega_2 t)}{k} \tag{1}$$

The first term is the fundamental sine wave. The 2nd term is subtracted from the first term to make gentler slope at the

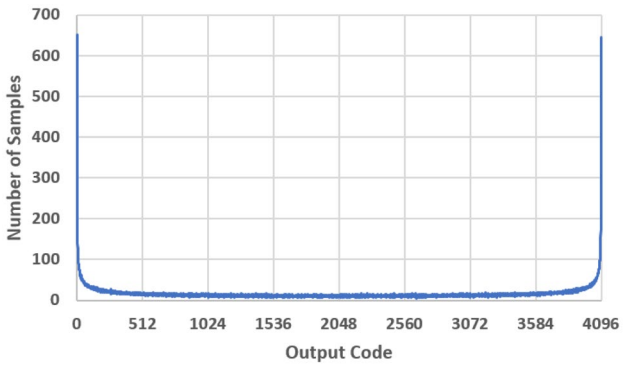

Fig. 5 Ideal 12-bit ADC output histogram for the sine wave input

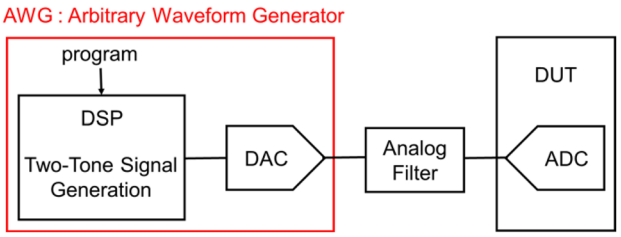

Fig. 6 Hardware components for generating proposed two-tone sine wave

codes which corresponds to the MSB bits to amplitude the bins around the codes.

The two-tone sine wave is generated by the arbitrary waveform generator (AWG) as shown in Fig. 6 [20, 22]. The arbitrary digital two-tone sine wave is generated from DSP. After the digital signal is converted to analog signal by DAC, it is applied to DUT through analog filter.

In the next subsection the detail is shown with some simulation results.

3.4 Simulation Results

To show the effectiveness of the proposed method, some simulation results are shown. In this simulation, 10-bit SAR ADC is assumed and thus the ADC output ranges from 0 to 1023. The number of samples is 2^{16}. The value of ω_1 of Eq. 1 is 1. The input range of the DUT is from -1 to 1. In general, the probability density function of the appearance of the codes is required to calculate DNL and INL. To calculate the probability density function, the inverse function of the test stimulus is required. However, it is difficult to obtain the inverse function of the two-tone sine wave. To solve the problem, DNL and INL of two-tone waveform is calculated with the method from [23] without use of the inverse function.

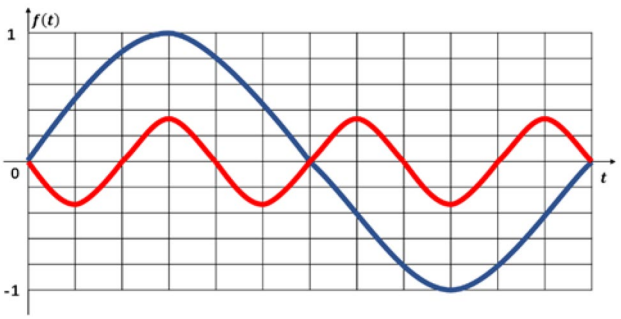

Fig. 7 Waveforms $f(t) = \sin(t)$ in blue and $f(t) = -\frac{\sin(3t)}{3}$ in red

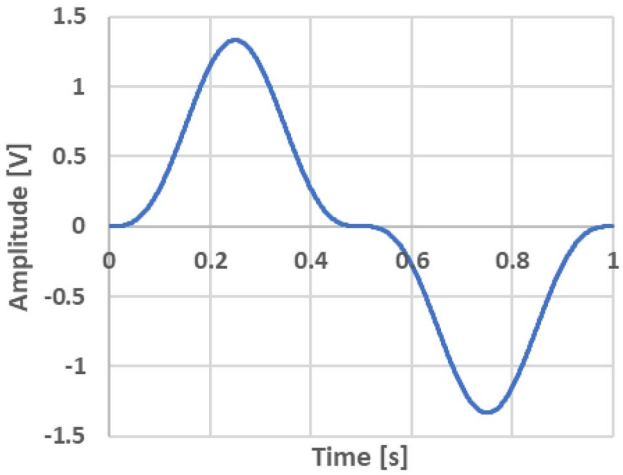

Fig. 8 Input wave $f_3(t) = \sin(t) - \frac{\sin(3t)}{3}$

3.4.1 Waveform, Histogram, DNL, and INL

The gentler the slope of the input signal waveform is, the more samples at the corresponding amplitude positions (codes) the obtained ADC output data has. Therefore, we consider to make the slope gentler at the corresponding amplitude positions by two-tone sine wave.

First, we consider increasing the number of samples around the center 512. Figure 7 plots the first term and second term of Eq. 2, respectively. The value of k is 3. The slope of $f_3(t)$ at the center is reduced to zero (t = arcsin0 = π) as shown in Fig. 8.

$$f_3(t) = \sin(t) - \frac{\sin(3t)}{3} \tag{2}$$

Figure 9 shows the histogram when the test stimulus of Eq. 2 is applied to the ideal 10-bit ADC.

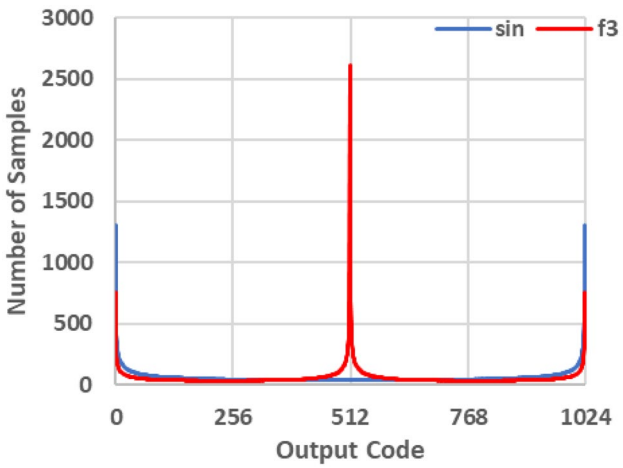

Fig. 9 Ideal 10-bit ADC output histogram for the input signal of $f_3(t) = \sin(t) - \frac{\sin(3t)}{3}$ in red and $f(t) = \sin(t)$ in blue

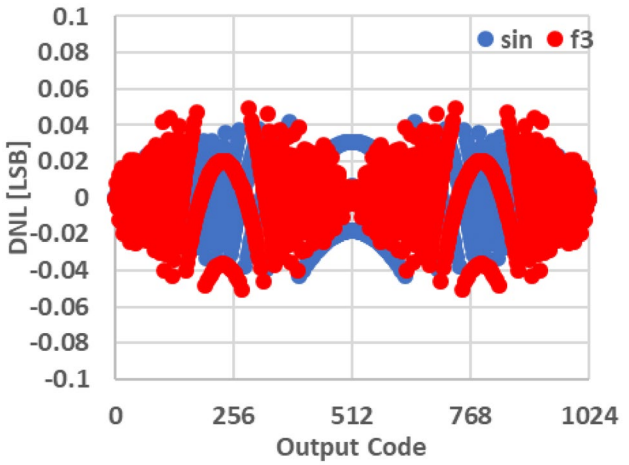

Fig. 10 Ideal 10-bit ADC DNL for the input signal of $f_3(t) = \sin(t) - \frac{\sin(3t)}{3}$ in red and $f(t) = \sin(t)$ in blue

As a result, we see that the number of samples near the center (near the digital output 512) is increased, as shown in Fig. 9.

Figures 10 and 11 show the obtained ideal 10-bit ADC DNL and INL measurements of the two-tone sine wave $f_3(t)$ and $\sin(t)$, respectively. The distributions of both the ideal 10-bit ADC DNL and INL of the two-tone sine wave become narrower around the code 512 where the length of the bin of the histogram is longer.

Next, we consider increasing the number of samples around 256 and 768. In other words, we adjust the amplitude positions to create more instances of gentle waveform slope; for example, $t = \arcsin\frac{1}{2} = \frac{\pi}{6}, \ldots$ Notice that $\frac{\pi}{6}$ is 1/12 of the period 2π, and each term of the two-tone sine wave of Eq. 3 is shown in Fig. 12. The value of k is 25. The waveform of the two-tone sine wave is shown in Fig. 13.

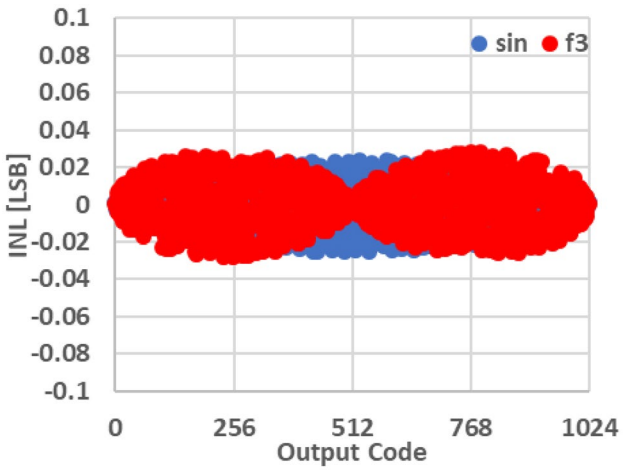

Fig. 11 Ideal 10-bit ADC INL for the input signal of $f_3(t) = \sin(t) - \frac{\sin(3t)}{3}$ in red and $f(t) = \sin(t)$ in blue

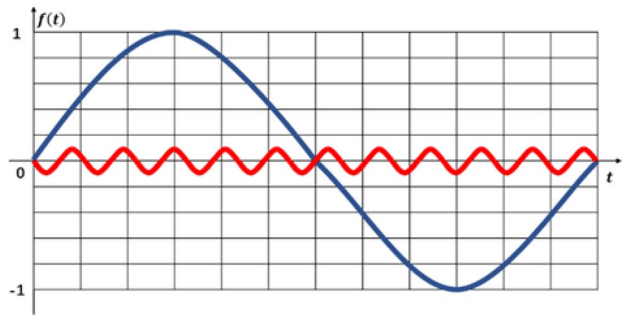

Fig. 12 f(t) = sin(*t*)in blue and f(t) = $-\frac{\sin(11t)}{25}$ in red.

$$f_{11}(t) = \sin(t) - \frac{\sin(11t)}{25} \tag{3}$$

Figure 14 shows the histogram when the test stimulus of Eq. 3 is applied to the ideal 10-bit ADC.

The number of samples near the targets (256, 768 as well as 512) has increased. The histogram has the sharp extra two peaks around the codes. These extra peaks occur around the maximum and minimum values of the fundamental sine wave because the slope of the fundamental sine wave of some of these areas is equal to or sometimes gentler than that of the second tone of the input two-tone sine wave. It sometimes gives bad effect to calculation of DNL and INL [23].

Figures 15 and 16 show the obtained ideal 10-bit ADC DNL and INL measurements of the two-tone sine wave $f_{11}(t)$ and $\sin(t)$, respectively. The distributions of both DNL and INL of the two-tone sine wave become narrower around the codes 256, 768 and 512 where the length of the bin of the histogram is longer.

Next, the proposed method is applied to a non-linear ADC to calculate the DNL. Here, relatively larger DNLs

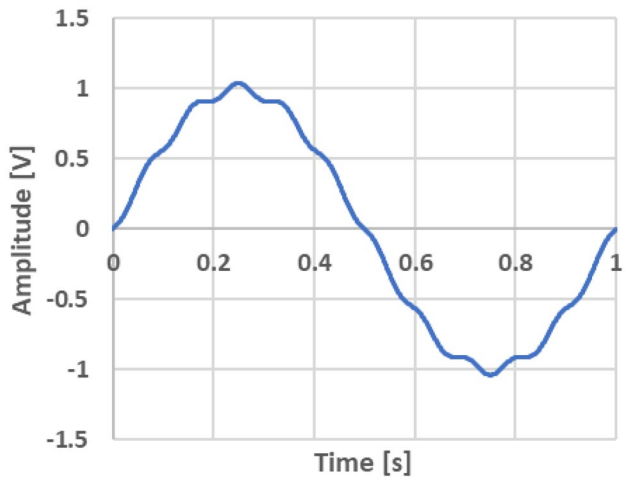

Fig. 13 Input wave $f_{11}(t) = \sin(t) - \frac{\sin(11t)}{25}$

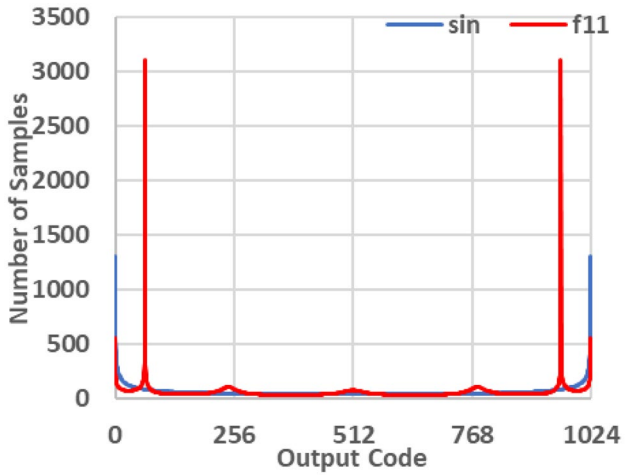

Fig. 14 Ideal 10-bit ADC output histogram for the input signal of $f_{11}(t) = \sin(t) - \frac{\sin(11t)}{25}$ in red and $f(t) = \sin(t)$ in blue

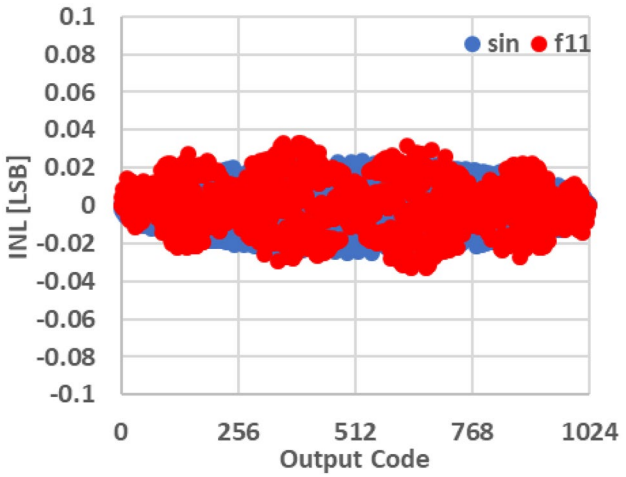

Fig. 16 Ideal 10-bit ADC INL for the input signal of $f_{11}(t) = \sin(t) - \frac{\sin(11t)}{25}$ in red and $f(t) = \sin(t)$ in blue

are added to the vulnerable 3 codes, 511, 255, 767, respectively and calculate the DNLs with the proposed method and the conventional sine wave method. In this evaluation, 0.94, -0.47, -0.47 (LSB) are added to the codes 511, 255, 767 as DNL, respectively. Table 1 shows the results. The 1st column is the output codes with relatively larger DNL. The 2nd column is the added DNL (LSB). The 3rd column is the DNL (LSB) by the proposed method and the error (LSB). The 4th column is the DNL (LSB) by the conventional sine wave method and the error (LSB). The errors of the proposed method are smaller than those of the conventional sine wave method. The proposed method estimated the DNLs of the vulnerable codes accurately.

In the same way, we can use $\arcsin\frac{1}{4} \approx \frac{\pi}{12}$ ($\frac{1}{24}$ of period 2π) to consider increasing 384, 640 and $\arcsin\frac{1}{8} \approx \frac{\pi}{25}(\frac{1}{50}$ of period 2π) to consider increasing 448, 576. The following Eqs. 4 and 5 are corresponding two-tone sine waves. The values of k are 50, 100, respectively.

$$f_{23}(t) = \sin(t) - \frac{\sin(23t)}{50} \tag{4}$$

$$f_{51}(t) = \sin(t) - \frac{\sin(51t)}{100} \tag{5}$$

However, extra peaks of the histogram of $f_{23}(t)$ and $f_{51}(t)$ cause serious problem to calculate DNL and INL. To remove the extra peaks, the two-tone sine wave is amplified, and ω_2 is tuned. As a result, the following two equations Eqs. 6 and 7 are used instead of Eqs. 4 and 5, respectively.

$$f_{31}(t) = 1.2\left(\sin(t) - \frac{\sin(31t)}{50}\right) \tag{6}$$

$$f_{59}(t) = 1.2\left(\sin(t) - \frac{\sin(59t)}{100}\right) \tag{7}$$

Figures 17 and 18 show each histogram. The number of samples near target codes 128, 256, 384, 512, 640, 768, 896 of histogram of Fig. 17 should be increased. They are codes corresponding to the DAC output voltages. However,

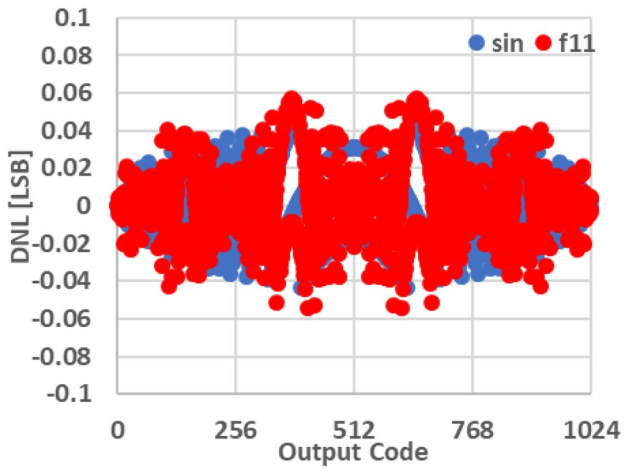

Fig. 15 Ideal 10-bit ADC DNL for the input signal of $f_{11}(t) = \sin(t) - \frac{\sin(11t)}{25}$ in red and $f(t) = \sin(t)$ in blue

Table 1 Calculation of DNL of ADC with non-linearity

output code	DNL	Proposed		sine wave	
		DNL	error	DNL	error
255	-0.47	-0.461	0.009	-0.490	-0.020
511	0.94	0.930	-0.010	0.914	-0.026
767	-0.47	-0.470	0.000	-0.447	0.023

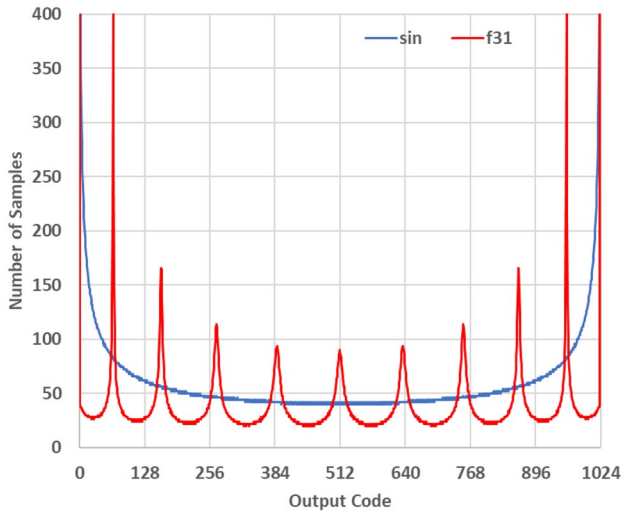

Fig. 17 Ideal 10-bit ADC output histogram for the input signal of $f_{31}(t) = 1.2\left(\sin(t) - \frac{\sin(31t)}{50}\right)$ in red and $f(t) = \sin(t)$ in blue

the peaks are not found on the codes 128, 256, 768, 896 in Fig. 17.

The number of samples near target codes 64, 128, 192, 256, 320, 384, 448, 512, 576, 640, 704, 768, 832, 896 of histogram of Fig. 18 should be increased. However, the peaks are not found on the codes 64, 128, 192, 832, 896 and 960 in Fig. 18. The heights of the peaks of the histograms of f_{31} and f_{59} are around 100. The widths of the peaks get narrower as ω_2 increases.

Figures 19, 20, 21 and 22 show the obtained ideal 10-bit ADC DNL and INL measurements of the two-tone sine waves $f_{31}(t)$ and $f_{59}(t)$, comparing with those of $\sin(t)$, respectively. Compared to the distributions of DNL and INL

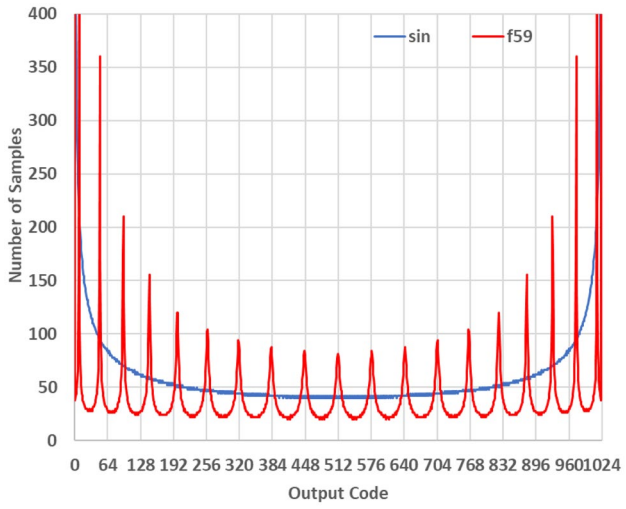

Fig. 18 Ideal 10-bit ADC output histogram for the input signal of $f_{59}(t) = 1.2\left(\sin(t) - \frac{\sin(59t)}{100}\right)$ in red and $f(t) = \sin(t)$ in blue

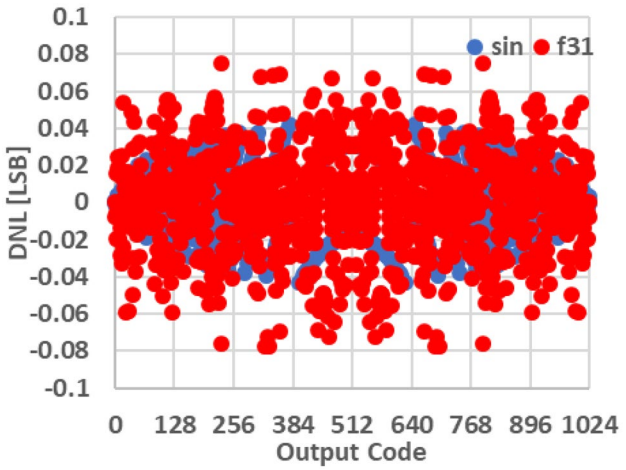

Fig. 19 Ideal 10-bit ADC DNL for the input signal of $f_{31}(t) = 1.2\left(\sin(t) - \frac{\sin(31t)}{50}\right)$ in red and $f(t) = \sin(t)$ in blue

$f_3(t)$ of $f_{11}(t)$, those of $f_{31}(t)$ and $f_{59}(t)$ spread relatively widely in the vertical direction.

The INL and DNL around the codes with high peak seems to be larger as the number of peaks increases.

3.4.2 Sensitivity of Histogram Shape

Next, we evaluate the sensitivity of the shape of the histogram to the variation of the level of the 2nd term of the two-tone sine wave. We observe how the shape of the histogram is varied when k is moved. In this evaluation, the angular frequency is fixed to 3 ω_1 or 11. In case that ω_2 is fixed to 3, the histograms of the ideal 10-bit ADC are obtained in the condition that $k = 3, 4, 5$. In case that is fixed to 11 ω_1, the histograms of the ideal 10-bit ADC are obtained in

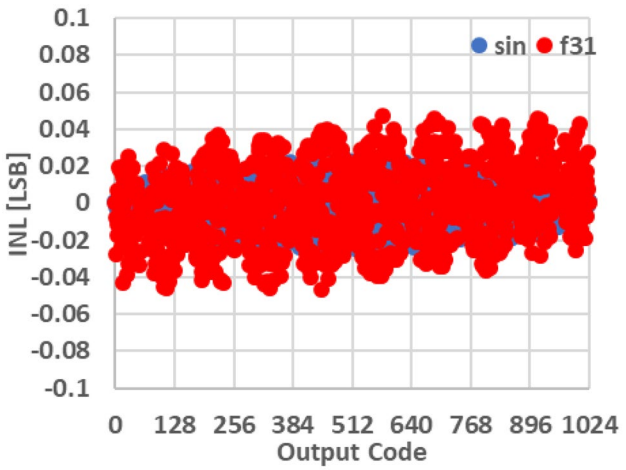

Fig. 20 Ideal 10-bit ADC INL for the input signal of $f_{31}(t) = 1.2\left(\sin(t) - \frac{\sin(31t)}{50}\right)$ in red and $f(t) = \sin(t)$ in blue

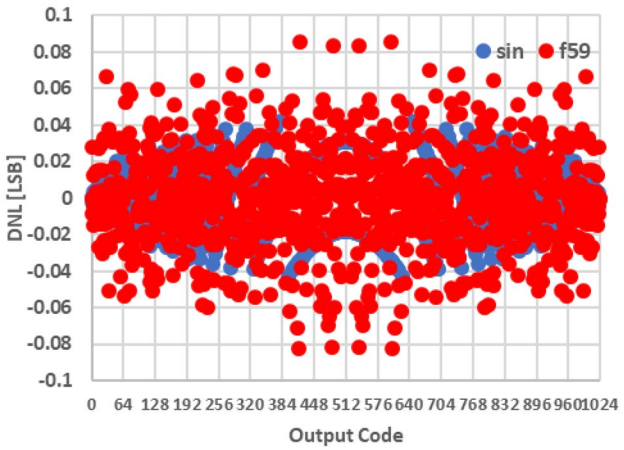

Fig. 21 Ideal 10-bit ADC DNL for the input signal of $f_{59}(t) = 1.2\left(\sin(t) - \frac{\sin(59t)}{100}\right)$ in red and $f(t) = \sin(t)$ in blue

the condition that. Figures 23 and 24 show the results. In both cases, the level of the peaks of the histograms becomes lower as k increases. On the other hand, the width of the peaks spreads as k increases.

3.4.3 Sensitivity of DNL, INL to Inaccuracy of Input Tones

Here, we evaluate how amplitude and phase error affects to the DNL and INL of the proposed method.

Following equation is used for the evaluation to consider the case that $\omega_2 = 3\omega_1, k = 3$ in Eq. 1.

$$f(t) = \sin(t) - A\sin(3t + \theta)/3$$

where A—1 is amplitude error, θ is phase error. When no error exists, $A = 1$, $\theta = 0$. Here we consider the case that

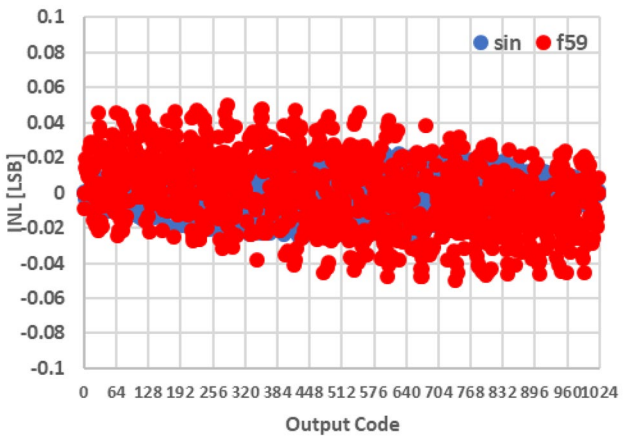

Fig. 22 Ideal 10-bit ADC INL for the input signal of $f_{59}(t) = 1.2\left(\sin(t) - \frac{\sin(59t)}{100}\right)$ in red and $f(t) = \sin(t)$ in blue

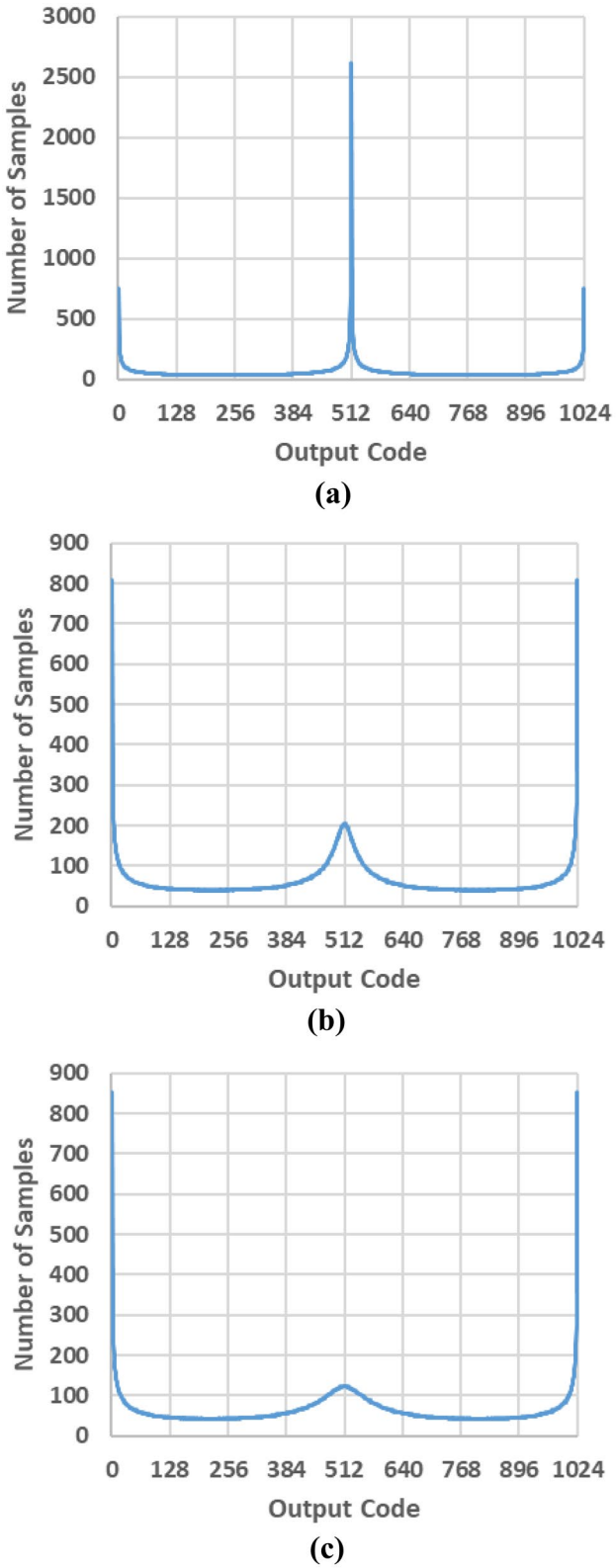

Fig. 23 Ideal10-bit ADC output histograms in case $\omega_2 = 3\omega_1$. (**a**) $k = 3$, (**b**) $k = 4$, (**c**) $k = 5$

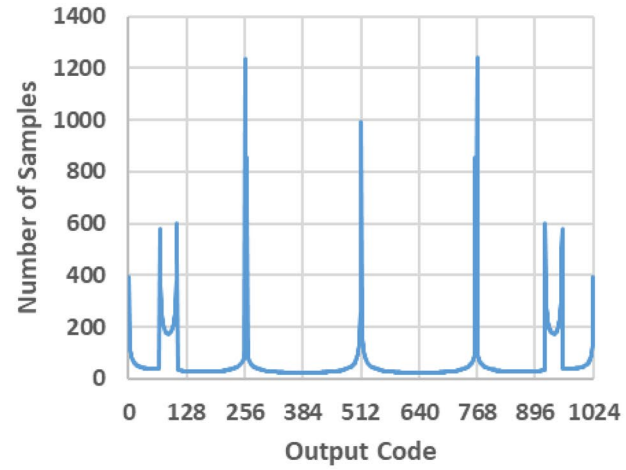

(a)

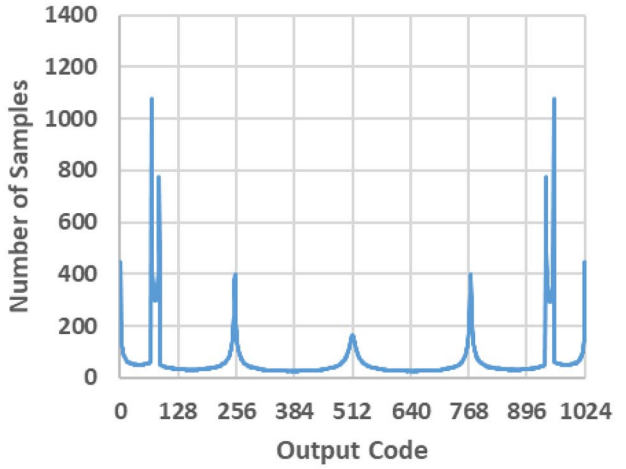

(b)

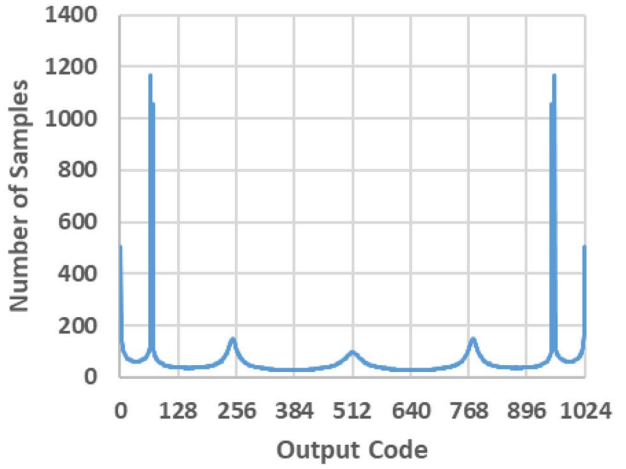

(c)

Fig. 24 Ideal10-bit ADC output histograms in case $\omega_2 = 11\omega_1$. (**a**) $k = 11$, (**b**) $k = 15$, (**c**) $k = 20$

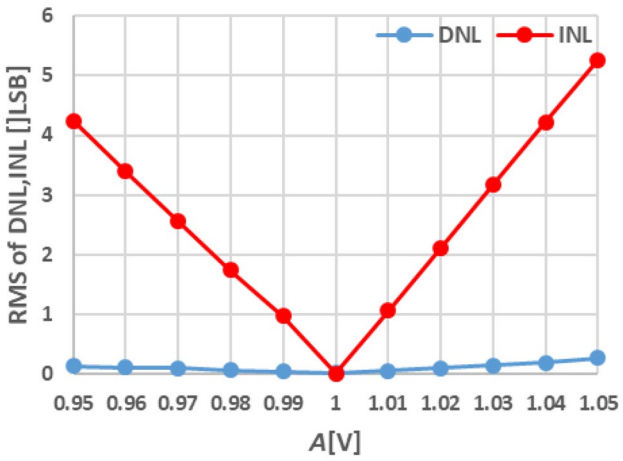

Fig. 25 Amplitude error characteristics of RMS of DNL, INL

$A \neq 1, \theta = 0$, where amplitude error exists. We calculate DNL and INL with the equation when $A = 1$, $\theta = 0$. From the calculated DNL and INL, the root mean square (RMS) of the DNL and INL is obtained. The RMS is calculated in case that $A = 0.95$, 0.96, 0.97, 0.98, 0.99, 1.0, 1.01, 1.02, 1.03, 1.04, 1.05.

Similarly, we consider the case that $A = 1, \theta \neq 0$, where phase error exists. We calculate DNL and INL with the equation when $A = 1$, $\theta = 0$. From the calculated DNL and INL, the RMS of the DNL and INL is obtained. The RMS is calculated in case that θ = -5, -4, -3, -2, -1, 0, 1, 2, 3, 4, 5(degree).

Figure 25 is amplitude error characteristics of the RMS of the DNL and INL. The horizontal axis is A, the vertical axis is the RMS of the DNL and INL. The curve of DNL is almost constant compared with the curve of INL. It is unsensitive to the amplitude error. On the other hand, the curve of INL is downward convex. It takes the maximum INL value near 5.2 with $A = 1.05$.

Figure 26 is phase error characteristics of the RMS of the DNL and INL. The horizontal axis is θ, the vertical axis is the RMS of the DNL and INL. The curve of DNL is almost constant compared with the curve of INL, although both of the shapes of the curves are downward convex with origin symmetry.

Regarding to these results, the amplitude error of INL is more sensitive than the others.

In practical applications, the condition would not be appropriate because the 3rd-order nonlinearity component of the DAC inside the AWG and that of the ADC under test would affect the component at the ADC output; sometimes, 3rd-order nonlinearity cannot be neglected. However, the input waveforms yielded by Eqs. (3), (6), (7) are useful

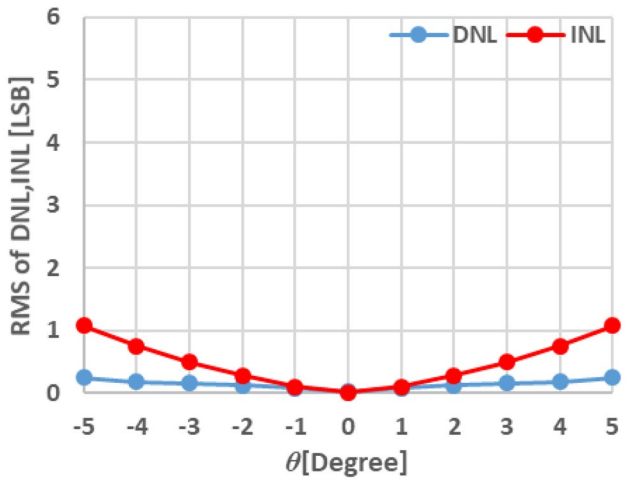

Fig. 26 Phase error characteristics of RMS of DNL, INL

because the 11th, 39th, and 51th order nonlinearities are usually very small.

4 Decision of Optimal Sampling Frequencies Based on Classical Mathematics

This section describes the decision method of the optimal sampling frequency of histogram method based on classical mathematics [26].

Here f_{sig}, f_{CLK} are defined as the input signal frequency and sampling frequency for histogram method, respectively.

Table 2 Metallic ratios

N	The n-th metallic number	Decimal expansion	Nickname
0	1		
1	$\frac{1+\sqrt{5}}{2}$	1.6180339887…	Golden ratio ∅
2	$1+\sqrt{2}$	2.4142135623…	Silver ratio
3	$\frac{3+\sqrt{13}}{2}$	3.3027756377…	Bronze ratio
4	$2+\sqrt{5}$	4.2360679774…	
…	…		
N	$\frac{n+\sqrt{n^2+4}}{2}$		

With these parameters, $T_{sig} = 1/f_{sig}$, $T_{CLK} = 1/f_{CLK}$ are also defined as the periods, respectively. With ignoring noise effect and initial phase difference between the frequencies, we can express the n-th sampling point of the sampling point's sequence p_n as follows.

$$p_n = nT_{CLK} mod\ T_{sig}$$

If the sequence distributes pseudo-randomly, accurate test result can be obtained with relatively small number of histogram data (in other words, with short test time). Accordingly, for accurate test, the ratio between f_{CLK} and f_{sig} is important.

We try to find the optimal f_{CLK}/f_{sig} with the following two data sampling methods. Subsections 4.1 and 4.2 explains these sampling methods, respectively. Subsection 4.3 gives the characteristics of each sampling method and compare them.

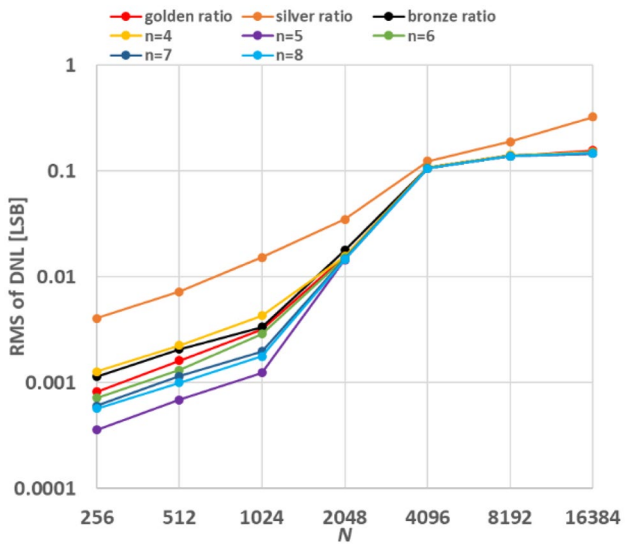

Fig. 27 Resolution characteristics of RMS of DNL of metallic ratio samplings (no noise)

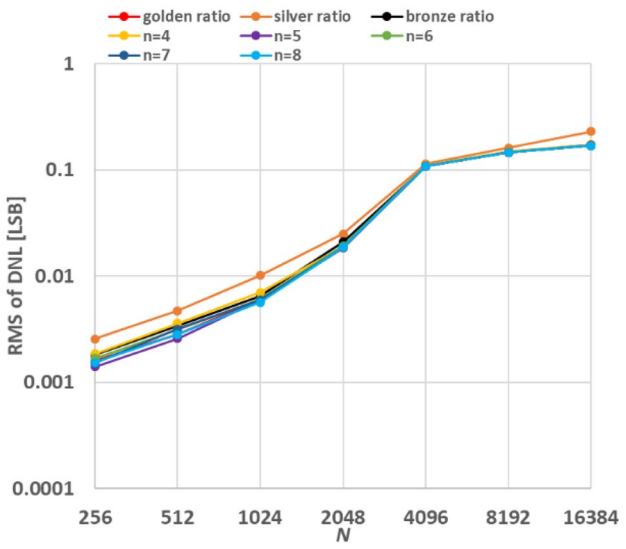

Fig. 28 Resolution characteristics of RMS of DNL of metallic ratio samplings (noise 0.001%)

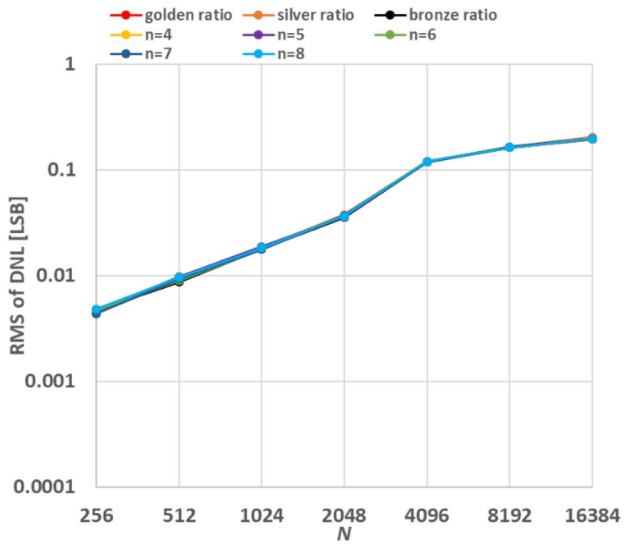

Fig. 29 Resolution characteristics of RMS of DNL of metallic ratio samplings (noise 0.01%)

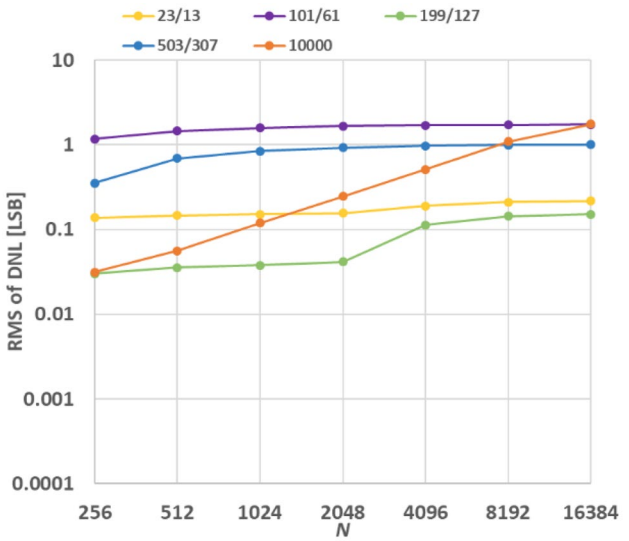

Fig. 31 Resolution characteristics of RMS of DNL of prime number ratio samplings by a pair of relatively smaller prime numbers (no noise)

Finally, some of the better samplings are compared with the real number sampling method.

4.1 Metallic Ratio Sampling

The first attempt is to introduce metallic ratio to the ratio between f_{CLK} and f_{sig}. As shown in Table 2, metallic ratio is defined as $M_n = (n + \sqrt{n^2 + 4})/2$. The sampling frequency of the metallic ratio sampling is decided as $f_{CLK} = M_n \times f_{sig}$. The metallic sampling can be performed keeping the ratio of the maximum and minimum distances between adjacent sampling points to be small. Also, the pseudo-randomness of the sampling points is improved approximately in proportional to the number of the data [23]. The authors investigated the relationship between f_{CLK} and f_{sig} and found that the "golden ratio" can effectively acquire the waveform in the time domain, and the proposed sampling condition ($f_{CLK} = \varnothing f_{sig}, \varnothing$: golden ratio) offers efficient waveform sampling, which we call golden ratio sampling [24, 25].

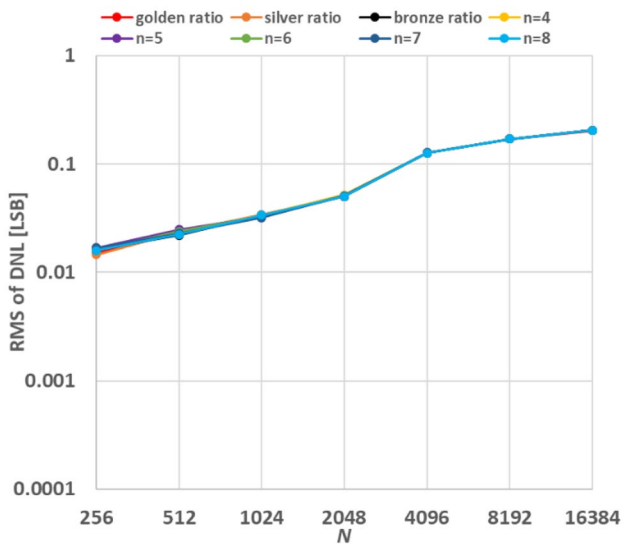

Fig. 30 Resolution characteristics of RMS of DNL of metallic ratio samplings (noise 0.1%)

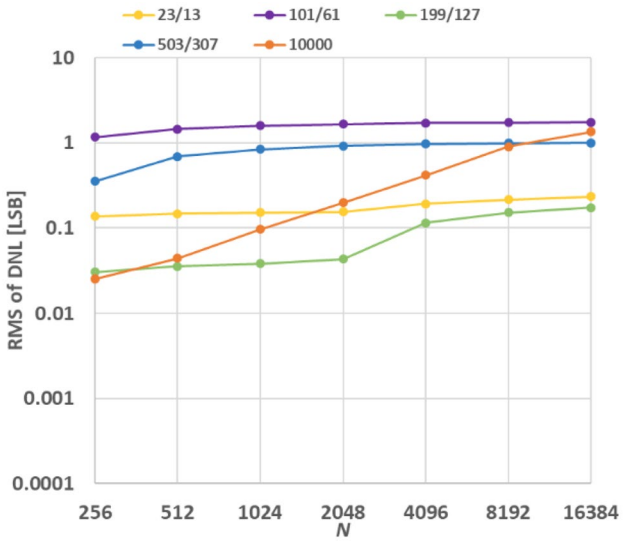

Fig. 32 Resolution characteristics of RMS of DNL of prime number ratio samplings by a pair of relatively smaller prime numbers (noise 0.001%)

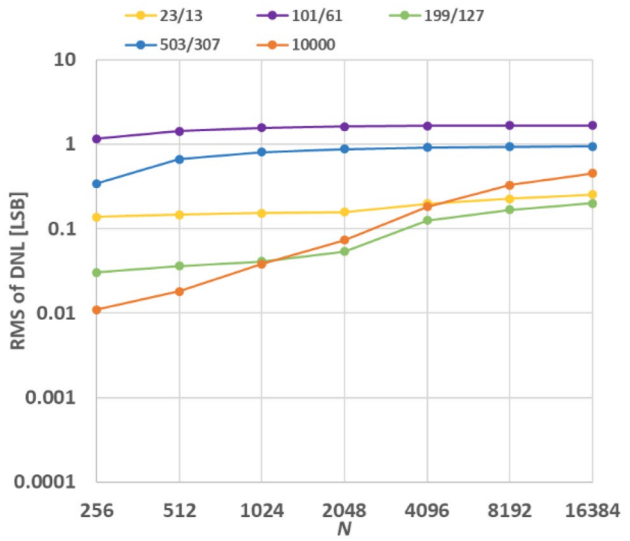

Fig. 33 Resolution characteristics of RMS of DNL of prime number ratio samplings by a pair of relatively smaller prime numbers (noise 0.01%)

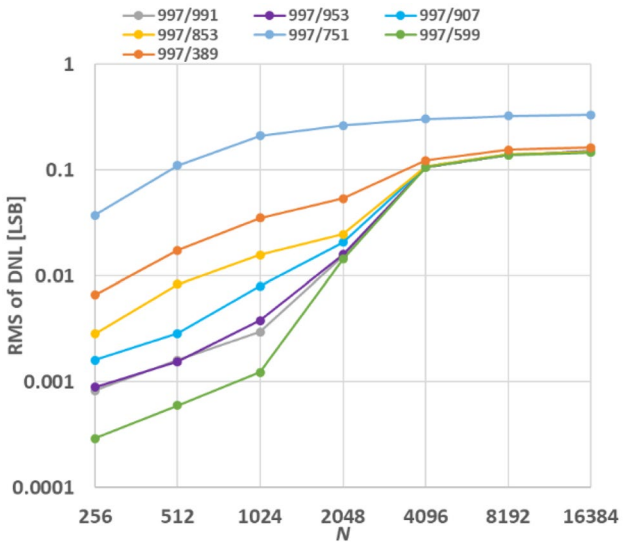

Fig. 35 Resolution characteristics of RMS of DNL of prime number ratio samplings by a pair of relatively larger prime numbers (no noise)

This paper applies the metallic ratio sampling to the ADC linearity test with histogram method, and investigate the characteristics.

4.2 Prime Number Ratio Sampling

The second attempt is to apply the prime number ratio sampling. Two prime numbers are used as ratios f_{CLK}/f_{sig} (such as 23/13, 101/61, 199/127, 503/507).

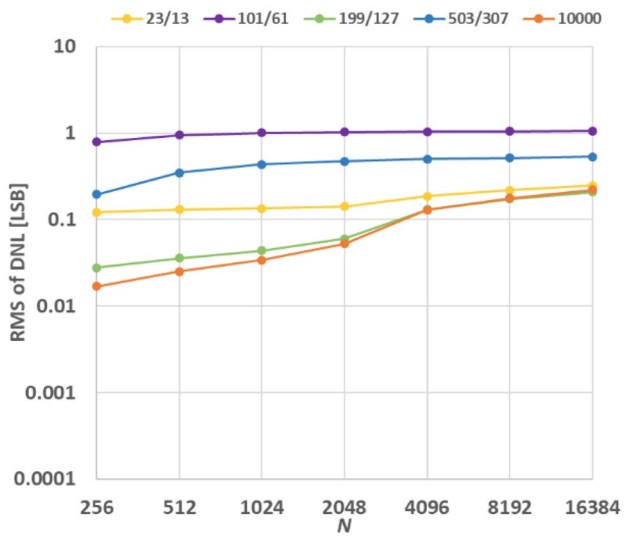

Fig. 34 Resolution characteristics of RMS of DNL of prime number ratio samplings by a pair of relatively smaller prime numbers (noise 0.1%)

4.3 Simulation Results

Simulation is performed to investigate the optimal sampling method for code selective histogram method. The criterion for the evaluation is RMS of DNL. The code selective histogram method is executed sweeping the resolution from 4 to 14 bit. In this evaluation, the two-tone sine wave of Eq. 3 is used. The number of samples M is 2^{20}. In each resolution, RMS of DNL is calculated. Then resolution characteristics

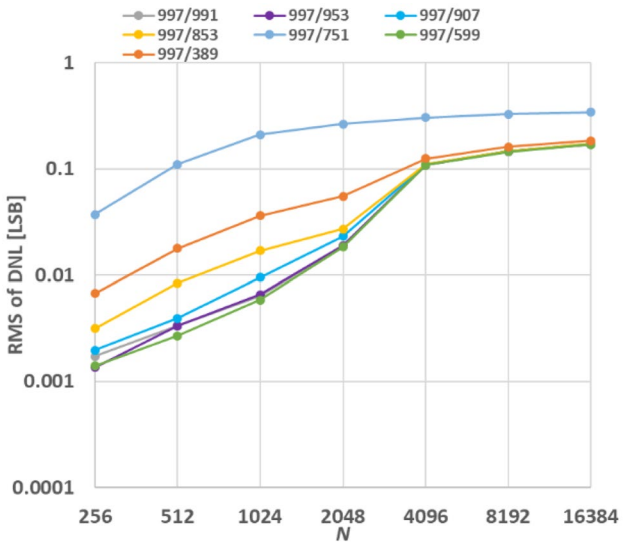

Fig. 36 Resolution characteristics of RMS of DNL of prime number ratio samplings by a pair of relatively larger prime numbers (noise 0.001%)

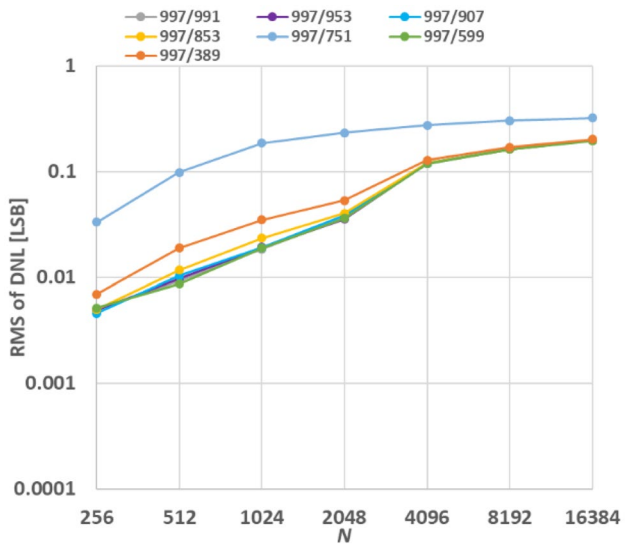

Fig. 37 Resolution characteristics of RMS of DNL of prime number ratio samplings by a pair of relatively larger prime numbers (noise 0.01%)

of RMS of DNL is obtained. The characteristics are obtained in each sampling method.

Subsubsection 4.3.1 evaluates the metallic ration sampling and Subsubsection 4.3.2 evaluates the prime number ratio sampling. Then the metallic ratio sampling is compared with the prime number ratio and real number ratio sampling. The detail of the real number ratio sampling is explained later.

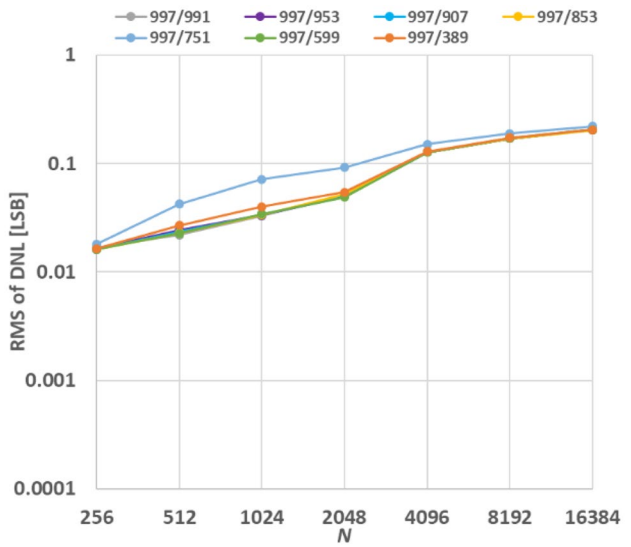

Fig. 38 Resolution characteristics of RMS of DNL of prime number ratio samplings by a pair of relatively larger prime numbers (noise 0.1%)

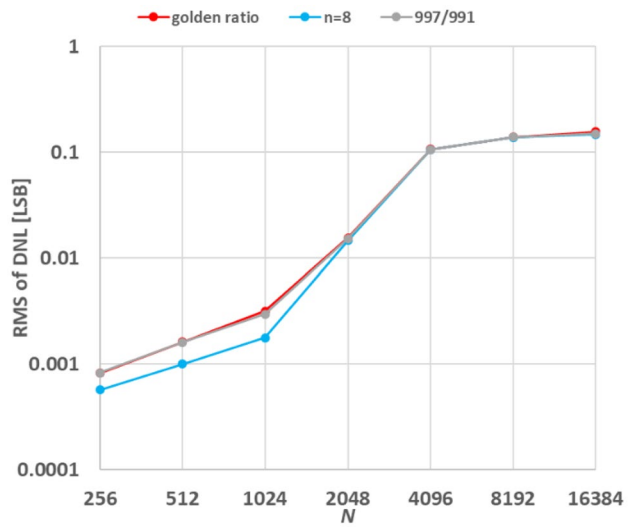

Fig. 39 Comparison of resolution characteristics of RMS of DNL of metallic ratio samplings with those of prime number ratio sampling (no noise)

4.3.1 Results of Metallic Ratio

In some cases of ADC testing, several frequencies of f_{sig} must be examined for a fixed f_{CLK}, or several frequencies of f_{CLK} for a fixed f_{sig}. In such cases, golden ratio sampling is inadequate, so we investigated more relationships between f_{CLK} and f_{sig}, using metallic ratios (Table 2). Notice that the golden ratio is one of the metallic ratios [27].

Resolution characteristics of RMS of DNL of metallic ratio sampling are obtained. In this evaluation, f_{CLK}

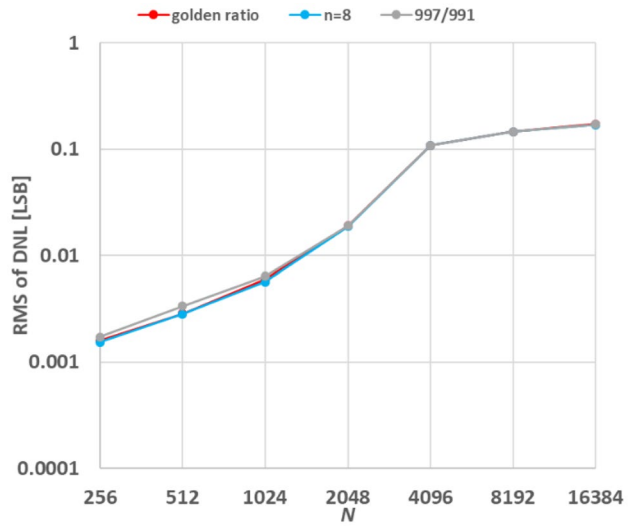

Fig. 40 Comparison of resolution characteristics of RMS of DNL of metallic ratio samplings with those of prime number ratio sampling (noise 0.001%)

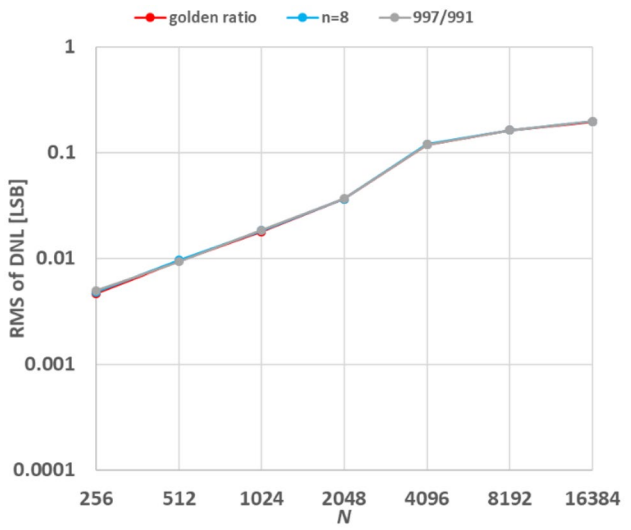

Fig. 41 Comparison of resolution characteristics of RMS of DNL of metallic ratio samplings with those of prime number ratio sampling (noise 0.01%)

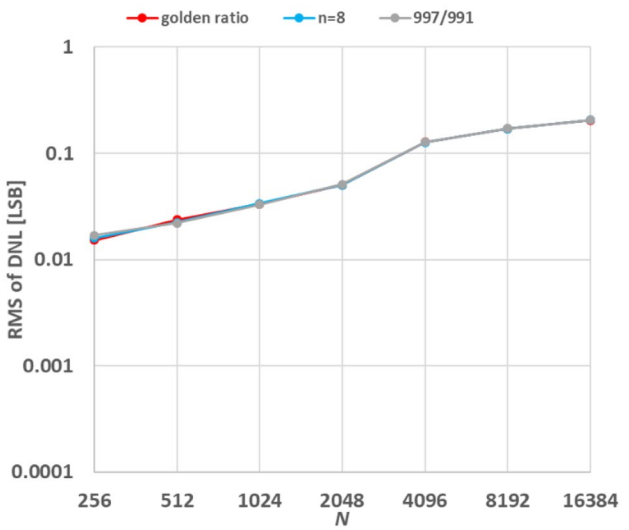

Fig. 42 Comparison of resolution characteristics of RMS of DNL of metallic ratio samplings with those of prime number ratio sampling (noise 0.1%)

$/f_{sig} = M_n$. The value n is varied from 1 to 8, and the resolution characteristics are evaluated in the 8 cases. The characteristics are obtained under both of the conditions without and with noise. In case of the condition with noise, Gaussian noise is added to the period of the fundamental sine wave of the two-tone test stimulus and the sampling period.

Figures 27, 28, 29, 30 show the characteristics without noise, with 0.001% Gaussian noise, with 0.01% Gaussian noise, with 0.1% Gaussian noise, respectively. The horizontal axis of each figure is division number N. The resolution of ADC is $\log_2 N$ (bits). The vertical axis is RMS of DNL.

In all the characteristics, RMS of DNL increases as N increases. It is because M/N decreases as N increases.

According to Fig. 27, The characteristics of M_2 namely Silver ratio are the worst, and all the characteristics except the case of M_2 are almost similar. The larger noise is, the worse characteristics are. The similarity of the characteristics becomes higher as the added noise increases.

4.3.2 Results of Prime Number Ratio

Resolution characteristics of RMS of DNL of prime number ratio sampling are obtained.

In this evaluation, two cases are evaluated: prime number ratio sampling by a pair of relatively small prime numbers and prime number ratio sampling by a pair of relatively large prime numbers. In the evaluation of prime number ratio samplings by a pair of relatively small prime numbers, the characteristics of the prime number samplings when f_{CLK}/f_{sig}= 23/13, 101/61, 199/127, 503/307 are evaluated. On the other hand, in the evaluation of prime number ratio samplings by a pair of relatively large prime numbers, the characteristics of the prime number samplings when f_{CLK}/f_{sig}= 997/991, 997/953, 997/907, 997/853, 997/751, 997/599, 997/389 are evaluated. Figures 31, 32, 33, 34 show the characteristics of the prime number ratio samplings by a pair of relatively small prime numbers without noise, with 0.001% Gaussian

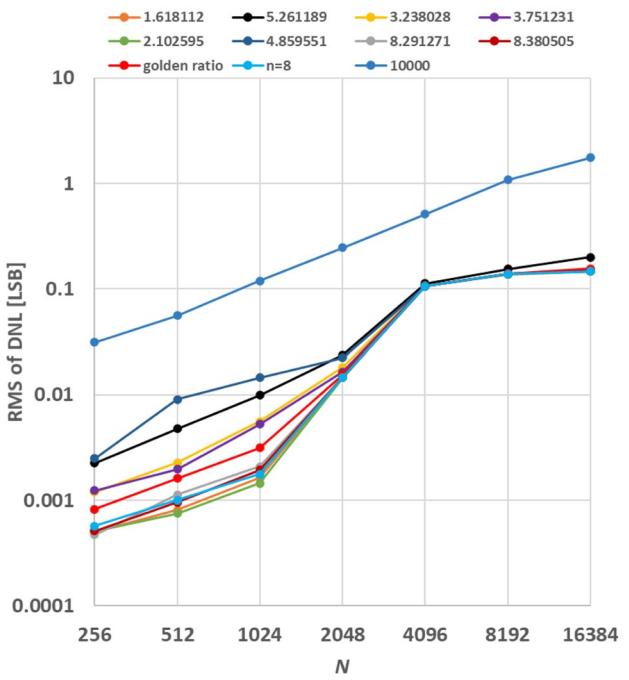

Fig. 43 Comparison of resolution characteristics of RMS of DNL of metallic ratio samplings with those of real number ratio sampling (no noise)

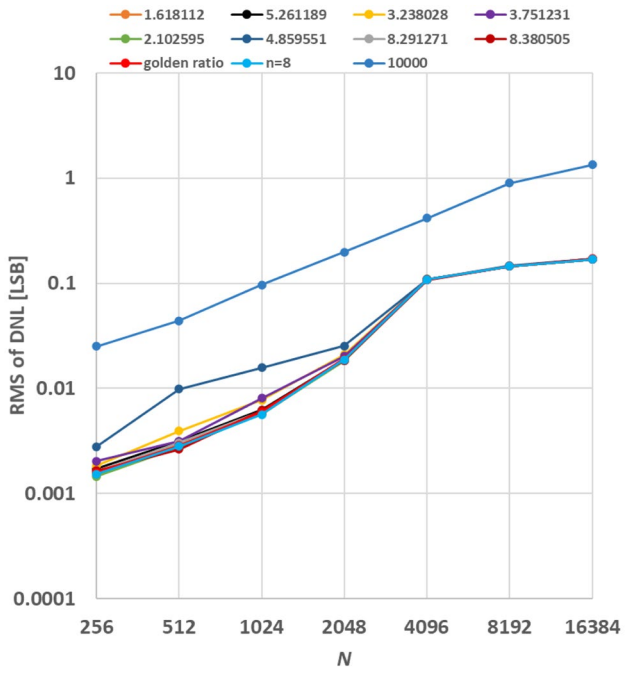

Fig. 44 Comparison of resolution characteristics of RMS of DNL of metallic ratio samplings with those of real number ratio sampling (noise 0.001%)

noise, with 0.01% Gaussian noise, with 0.1% Gaussian noise, respectively. Overall, the results of Fig. 31 of the prime number samplings by a pair of relatively small prime numbers have poor characteristics compared with those of Fig. 27 of the metallic ratio samplings. Especially, the RMS of DNL of 101/61 is more than 1.

The characteristics largely depend on the pair of the values of the prime numbers. The curves spread relatively widely in the vertical axis direction.

The prime number ratio samplings are compared with the case when the ratio is 10000 where $f_{CLK} \gg f_{sig}$. The rate of increase in characteristics is larger compared with the other characteristics. The minimum value taken at $N = 256$ is close to the value of 199/127. The maximum value taken at $N = 16{,}384$ is closes to the value of 101/61.

As the noise increases, the characteristics of the prime number ratio samplings deteriorate overall and the spread of the curves in the vertical axis gradually narrows. On the other hand, the characteristics of 10,000 gradually improve with the increase of noise.

Figures 35, 36, 37, 38 show the characteristics of the prime number ratio samplings by a pair of relatively large prime numbers without noise, with 0.001% Gaussian noise, with 0.01% Gaussian noise, with 0.1% Gaussian noise, respectively.

According to Fig. 35, on the lower domain where N is less than 4096, the curves spread relatively widely in the vertical axis direction as well as the curves of the prime number ratio samplings by a pair of relatively small prime numbers. However, on the higher domain where N is more than 4096, the curves narrow. As the noise increases, the characteristics deteriorate overall and the spread of the curves in the vertical axis gradually narrows.

Two metallic ratio samplings M_1 (golden ratio sampling) and M_8 with relatively good characteristics are compared with the prime number ratio sampling $f_{CLK}/f_{sig} = 997/991$ with the best characteristics in the evaluation of the prime number ratio samplings. Figures 39, 40, 41, 42 show the characteristics of these samplings, with 0.001% Gaussian noise, with 0.01% Gaussian noise, with 0.1% Gaussian noise, respectively.

According to Fig. 39, these three samplings have almost same characteristics. The larger noise is, the worse characteristics are. The similarity of the characteristics becomes higher as the added noise increases.

Here, let us call the sampling using the real number as the ratio f_{CLK}/f_{sig} the real number ratio sampling.

Finally, two metallic ratio samplings M_1 (golden ratio sampling) and M_8 with relatively good characteristics are compared with the real number ratio samplings. In this evaluation, 8 real numbers in the range 1 to 10 where $M_n s (1 \le n \le 8)$ exist are generated randomly as the ratios for the real number ratio samplings. Figures 43, 44, 45, 46 show the characteristics of these samplings, with 0.001% Gaussian noise, with 0.01% Gaussian noise, with 0.1% Gaussian noise, respectively. The characteristics of the case

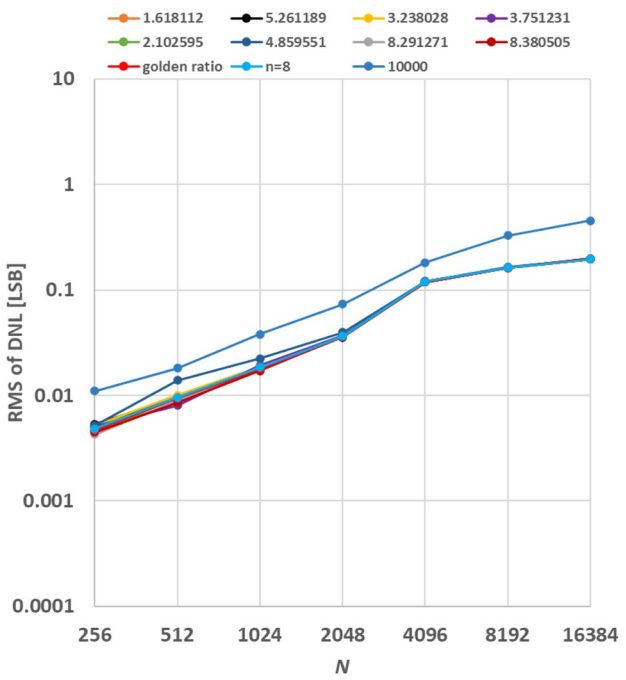

Fig. 45 Comparison of resolution characteristics of RMS of DNL of metallic ratio samplings with those of real number ratio sampling (noise 0.01%)

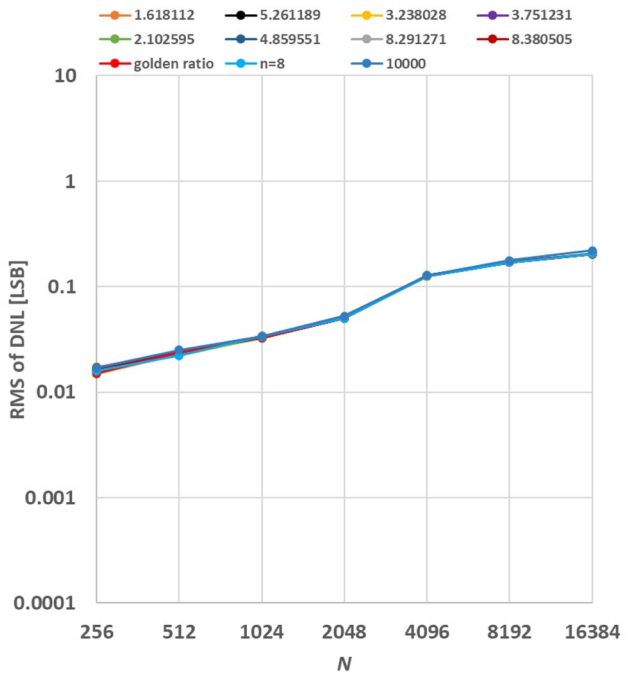

Fig. 46 Comparison of resolution characteristics of RMS of DNL of metallic ratio samplings with those of real number ratio sampling (noise 0.1%)

when $f_{CLK}/f_{sig} = 10000$ are plotted on the same planes as the case where $f_{CLK} \gg f_{sig}$. According to Fig. 43, on the lower domain where N is less than 4096, the curves spread relatively widely in the vertical axis direction compared to the higher domain where N is more than 4096. The characteristics of the two metallic ratio sampling are relatively better among all the characteristics of Fig. 43. It can be said that the characteristics of the real number ratio sampling are similar to the characteristics of the metallic ratio sampling. Compared to the characteristics of the case when $f_{CLK}/f_{sig} = 10000$, all the other characteristics are better. Like the characteristics of the other sampling methods, the similarity of the characteristics becomes higher as the added noise inc reases.

5 Conclusion

This article introduced a relatively simple method of focusing histogram sampling on specific codes. Our proposal synthesizes a two-tone wave to achieve rapid ADC linearity test. Simulations verified the validity of the proposed code selective histogram method and its good performance.

Using simulations, we examined several ratios such as metallic ratios and prime number ratios, between the input signal frequency and the sampling frequency, and found several interesting results.

For the case of small N, the performance achieved with the metallic ratios are similar in specific positions (32, 64, 128, 256, …).

These results can be used to obtain higher test accuracy with a small number of samples. We conclude this paper by remarking that the histogram method for the ADC linearity test is a mature technology, and it is widely used in industry, however, even in such a mature technology, there can be new algorithms and findings; these results are seen as industry friendly.

Data Availability Statement Authors can confirm that all relevant data are included in the article.

Declarations

Conflict of Interest There is no conflict of interest.

References

1. Kobayashi H, Kuwana A, Wei J, Zhao Y, Katayama S, Tri TM, Hirai M, Nakatani T, Hatayama K, Sato K, Ishida T (2020) Analog/Mixed-Signal Circuit Testing Technologies in IoT Era. IEEE 15th Int Conf Solid-State and Integrated Circuit Technol Kunming, China
2. Burns M, Roberts GW (2011) Burns, An Introduction to Mixed-Signal IC Test and Measurement, Oxford Press
3. Maloberti F (2007) Data Converters, Springer
4. IEEE (2011) IEEE Standard for Terminology and Test Methods for Analog-to-Digital Converters. In: IEEE Standard 1241–2010 (Revision IEEE Standard 1241–2000)
5. Jin L, Chen D, Geiger R (2005) A Digital Self-Calibration Algorithm for ADCs Based on Histogram Test Using Low-Linearity Input Signals. IEEE Int Symp Circuits Sys
6. Flore MG, Negreiros M, Carro L (2004) INL and DNL Estimation based on Noise for ADC Test. IEEE Trans Instrum Meas 53:1391–1395
7. Blair J (1994) Histogram Measurement of ADC Nonlinearities Using Sine Waves. IEEE Trans Instrum Meas 43:373–383
8. Ting H-W, Liu B-D, Chang S-J (2008) A Histogram-Based Testing Method for Estimating A/D Converter Performance. IEEE Trans Instrum Meas 57(2):420–427
9. Goyal S, Chatterjee A, Atia M, Iglehart H, Chen CY, Shenouda B, Khouzam N, Haggag H (2005) Test Time Reduction of Successive Approximation Register A/D Converter by Selective Code Measurement. IEEE Int Test Conference, Austin, TX
10. Goyal S, Chatterjee A (2008)Linearity Testing of A/D Converters Using Selective Code Measurement. J Electronic Testing, Springer
11. Yu Z, Chen D (2012) Algorithm for Dramatically Improved Efficiency in ADC Linearity Test," Proc. IEEE Int Test Conf 1–10
12. Chen T, Jin X, Geiger RL, Chen D (2018) "USER-SMILE: Ultra-fast Stimulus Error Removal and Segmented Model Identification of Linearity Errors for ADC Built-In Self-Test," IEEE Trans. Circuits Syst - Part I 65(7):2059–2069
13. Laraba A, Stratigopoulos H-G, Mir S, Naudet H (2015) "Exploiting Pipeline ADC Properties for a Reduced-Code Linearity Test Technique," IEEE Trans. Circuits Syst - Part I 62(10):2391–2400

14. Renaud G, Barragan MJ, Laraba A, Stratigopoulos H-G, Mir S, Le-Gall H, Naudet H (2016) A 65nm CMOS Ramp Generator Design and its Application Towards a BIST Implementation of the Reduced-Code Static Linearity Test Technique for Pipeline ADCs. J Electron Test 32:407–421
15. Feitoza RS, Barragan MJ, Mir S, Dzahini D (2018) Reduced-Code Static Linearity Test of SAR ADCs Using a Built-In Incremental $\sum\Delta$ Converter. Proc. IEEE 24th Int Symp On-Line Testing And Robust Sys Design (IOLTS) 29–34
16. Feitoza RS, Barragan MJ, Dzahini D, Mir S (2019) Reduced-Code Static Linearity Test of Split-Capacitor SAR ADCs Using an Embedded Incremental Sigma Delta Converter. IEEE Trans Device Mater Reliab 19(1):37–45
17. Huang XL, Chen HI, Huang JL, Chen CY, Kuo-Tsai T, Huang MF, Chou YF, Kwai DM (2012) Testing and Calibration of SAR ADCs by MCT-Based Bit Weight Extraction. IEEE 18th Int Mixed-Signal, Sensors, and Sys Test Workshop 1–4
18. Hirai M, Tanimoto H, Gendai Y, Yamamoto S, Kuwana A, Kobayashi H (2021) Digital-to-Analog Converter Configuration Based on Non-uniform Current Division Resistive-Ladder. The 36th Int Technical Conf Circuits/Systems, Comp Comm Korea
19. Hirai M, Tanimoto H, Gendai Y, Yamamoto S, Kuwana A, Kobayashi H (2020) Nonlinearity Analysis of Resistive Ladder-Based Current-Steering Digital-to-Analog Converter. 17th Int SoC Design Conf Yeosu, Korea
20. Abe F, Kobayashi Y, Sawada K, Kato K, Kobayashi O, Kobayashi H (2014) Low-Distortion Signal Generation for ADC Testing. IEEE Int Test Conf Seattle, WA
21. Komuro T, Sobukawa S, Sakayori H, Kono M, Kobayashi H (2007) Total Harmonic Distortion Measurement System for Electronic Devices up to 100MHz with Remarkable Sensitivity. IEEE Trans Instrum Meas 56(6):2360–2368
22. Uemori S, Yamaguchi T, Ito S, Tan Y, Kobayashi H, Takai N, Niitsu K, Ishikawa N (2010) ADC Linearity Test Signal Generation Algorithm. IEEE Asia Pacific Conf Circuits and Sys Kuala Lumpur, Malaysia
23. Ozawa Y, Kuwana A, Asami K, Kobayashi H (2019) ADC Linearity Testing Using Multi-tone Input Histogram Method. ETG-19–24, ETT-19–24, 9-th IEEJ Workshop in Tochigi and Gunma
24. Yamamoto S, Sasaki Y, Zhao Y, Wei J, Kuwana A, Sato K, Ishida T, Okamoto T, Ichikawa T, Nakatani T, Tran TM (2021) Metallic Ratio Equivalent-Time Sampling: A Highly Efficient Waveform Acquisition Method. 27th IEEE Int Symposium on On-Line Testing and Robust Sys Design Virtual event
25. Sasaki Y, Zhao Y, Kuwana A, Kobayashi H (2018) Highly Efficient Waveform Acquisition Condition in Equivalent-Time Sampling System. 27th IEEE Asian Test Symposium, Hefei, Anhui, China
26. Zhao Y, Kuwana A, Yamamoto S, Sasaki Y, Kobayashi H, Tran TM, Katayama S, Wei J, Nakatani T, Hatayama K, Sato K (2021) Input Signal and Sampling Frequencies Requirements for Efficient ADC Testing with Histogram Method. The 36th Int Technical Conf Circuits/Sys Comp Comm, Korea
27. Dickson LE (2005) History of the Theory of Numbers, vol. 2, Diophantine Analysis, Dover

Yujie Zhao completed the master's program (electronic information and mathematics) at Gunma University Graduate School in March 2020. He is currently enrolled in the doctoral program.

Kentaroh Katoh received the B.E. and M.E. degrees from Nagoya University, Nagoya, Japan, in 1997 and 1999, respectively, and the Ph.D. degree from Chiba University, Chiba, Japan, in 2009. In 1999, he joined Fujitsu Limited and engaged in the development of the embedded control system of HDD from 1999 to 2001. He joined Chiba University, in 2001. He worked in Tsuruoka National College of Technology as an Associate Professor from 2011 to 2018. He is currently a cooperative researcher at Division of Electronics and Informatics in Gunma University.

Anna Kuwana graduated from the Department of Computer Science, Faculty of Science, Ochanomizu University in March 2006, and completed the master's program at the same graduate school in September 2007. She received her PhDat the same graduate school in September). After working as a lecturer at Ochanomizu University, she became an assistant professor at the Division of Electronics and Informatics, Faculty of Science and Technology, Gunma University. She is engaged in research and education on computational fluid dynamics.

Shogo Katayama completed the master's program at Gunma University Graduate School in September 2020 (electronicinformation and mathematics). He is currently enrolled inthe doctoral program.

Jianglin Wei completed the master's program at Gunma University Graduate School in September 2019 (electronic information and mathematics). He is currently enrolled in the doctoral program.

Haruo Kobayashi received the B.S. and M.S. degrees in information physics from The University of Tokyo, Tokyo, Japan, in 1980 and 1982, respectively, an M.S. degree in electrical engineering from the University of California at Los Angeles, Los Angeles, CA, USA, in 1989, and thePh.D. degree in electrical engineering from Waseda University, Tokyo, in 1995. After working at Yokogawa Electric, he is currently a professor at the Department of Electronic Information, Graduate School of Science and Technology, Gunma University. He is engaged in research and education on analog and mixed signal LSI design, test facilitation, power supply circuits, and signal processing algorithms. He received the 2002 Yokoyama Science and Technology Award.

Takayuki Nakatani graduated from Waseda University, Faculty of Science and Engineering, Department of Telecommunications in 1974. He joined Takeda Riken Kogyo (renamed Advantest Co., Ltd.) in 1974 and worked on development and management of analog technology related to electronic measuring instruments, semiconductor test systems and electron beam exposure equipment. In 2003, he became Representative Director of Advantest Academy Co., Ltd. He is also a part-time lecturer in the Faculty of Science and Technology, Gunma University, and a part-time lecturer in the Faculty of Science and Technology, Tokyo Denki University.

Kazumi Hatayama received his B.S., M.S. and Ph.D.degrees in applied mathematics and physics from KyotoUniversity, Kyoto, Japan, in 1976, 1978 and 1982,respectively.He is now a cooperative researcher at Division ofElectronics and Informatics in Gunma University, after having engaged in research and development of test design automation technologies at Hitachi, Renesas and STARC,and of dependable VLSI solutions utilizing test technologies at NAIST.He is a senior member of IEEE and IEICE, and a member of IPSJ, REAJ and ORSJ.His research interests include DFT, BIST, ATPG, fault diagnosis and dependable systems.

Keno Sato received the B.S. degree in electrical engineering from Tokyo University of Science in 1999. Currently, He is a manager at ROHM Semiconductor and is working on testing of high-performance IP cores such as high accuracy OP-amplifier, analog-to-digital converter, voltage reference, etc., pursuing the most efficient analog test methodology.

Takashi Ishida received the B.S. degree in electrical engineering from Kindai University in 2007, and is presently an engineer at Rohm Co., Ltd. He has worked on test development for analog front-end devices.

Toshiyuki Okamoto received the B.S. degree in electronics engineeringfrom Doshisha University in 2009, and is presently an engineer at Rohm Co., Ltd. He has worked on test development for the analog-to-digital converter.

Tamotsu Ichikawa received the B.S. degree in electrical engineering from Meiji University in 2011, and is presently an engineer at Rohm Co., Ltd. He has worked on automation system development for the LSI test environment.